

# A Dichotomy in Satellite Quenching Around $L^*$ Galaxies

John I. Phillips,<sup>1\*</sup> Coral Wheeler,<sup>1</sup> Michael Boylan-Kolchin,<sup>1,2†</sup> James S. Bullock,<sup>1</sup>  
 Michael C. Cooper,<sup>1</sup> Erik J. Tollerud<sup>3‡</sup>

<sup>1</sup>centre for Cosmology, Department of Physics and Astronomy, 4129 Reines Hall, University of California, Irvine, CA 92697, USA

<sup>2</sup>Department of Astronomy, University of Maryland, College Park, MD 20742, USA

<sup>3</sup>Astronomy Department, Yale University, P.O. Box 208101, New Haven, CT 06510, USA

1 November 2018

## ABSTRACT

We examine the star formation properties of bright ( $\sim 0.1 L^*$ ) satellites around isolated  $\sim L^*$  hosts in the local Universe using spectroscopically confirmed systems in the Sloan Digital Sky Survey DR7. Our selection method is carefully designed with the aid of  $N$ -body simulations to avoid groups and clusters. We find that satellites are significantly more likely to be quenched than a stellar mass-matched sample of isolated galaxies. Remarkably, this quenching occurs only for satellites of hosts that are themselves quenched: while star formation is unaffected in the satellites of star-forming hosts, satellites around quiescent hosts are more than twice as likely to be quenched than stellar-mass matched field samples. One implication of this is that whatever shuts down star formation in isolated, passive  $L^*$  galaxies also plays at least an indirect role in quenching star formation in their bright satellites. The previously-reported tendency for “galactic conformity” in colour/morphology may be a by-product of this host-specific quenching dichotomy. The Sérsic indices of quenched satellites are statistically identical to those of field galaxies with the same specific star formation rates, suggesting that environmental and secular quenching give rise to the same morphological structure. By studying the distribution of pairwise velocities between the hosts and satellites, we find dynamical evidence that passive host galaxies reside in dark matter haloes that are  $\sim 45\%$  more massive than those of star-forming host galaxies of the same stellar mass. We emphasize that even around passive hosts, the mere fact that galaxies become satellites does not typically result in star formation quenching: we find that only  $\sim 30\%$  of  $\sim 0.1 L^*$  galaxies that fall in from the field are quenched around passive hosts, compared with  $\sim 0\%$  around star forming hosts.

**Key words:** galaxies: evolution – galaxies: dwarf – galaxies: quenching – cosmology: observations

## 1 INTRODUCTION

In the now-favored dark energy plus cold dark matter ( $\Lambda$ CDM) cosmological model, the abundance of dark matter subhaloes as a function of parent dark matter halo mass is predicted with high precision in  $N$ -body simulations (e.g. Boylan-Kolchin et al. 2009; Klypin, Trujillo-Gomez & Primack 2011). In contrast, the observed abundance and properties of satellite galaxies in the local Universe are poorly understood within the current cosmological framework. For example, modern semi-analytic (e.g. Somerville et al. 2008; Guo et al. 2011) and hydrodynamic (e.g. Davé, Oppen-

heimer & Finlator 2011) models of galaxy formation are overly effective at halting star formation in satellite systems, such that current models dramatically overpredict the number density of quenched (or passive) satellites at  $z \sim 0$  (Kimm et al. 2009; Weinmann et al. 2006, 2010, 2012).

Additionally, current models of galaxy formation fail to reproduce the relationship between host and satellite galaxy properties. In particular, recent studies of satellite and central galaxies in the Sloan Digital Sky Survey (SDSS, York et al. 2000) find that satellites of red (or passive) host galaxies are more likely to also be passive relative to their counterparts around star-forming hosts (Weinmann et al. 2006). This correlation between host and satellite properties, commonly dubbed “galactic conformity,” is also poorly replicated by modern semi-analytic models (Kauffmann et al. 2013), potentially due to a lack of decoupling between the

\* e-mail: johnip@uci.edu

† centre for Galaxy Evolution Fellow

‡ Hubble Fellow

growth of satellite galaxies and the growth of their dark matter haloes in the models (Weinmann et al. 2012). Ultimately, understanding this connection between the properties of host and satellite galaxies may be a powerful way to constrain the physical mechanisms responsible for halting star formation in passive systems.

To better understand the physics driving the relationship between the properties of host and satellite galaxies, it is particularly interesting to examine the satellite populations around  $L^*$  hosts. At this luminosity (or stellar mass), central galaxies are roughly equally likely to be star forming or quenched, while at higher (or lower) luminosities, the host population is increasingly dominated by passive (or star forming) systems (e.g. Kauffmann et al. 2003; Bell et al. 2003; Baldry et al. 2004). As such, this scale ( $\sim L^*$ ) is well-suited for exploring connections between host and satellite properties. Moreover, our own Milky Way falls into this class of galaxies; understanding the statistical properties of  $L^*$  galaxies will therefore inform our understanding of the Milky Way and its satellites, the objects that can be studied in the most detail.

In this work, we investigate satellite quenching mechanisms by comparing satellites around isolated  $L^*$  galaxies to a statistically identical sample of field galaxies. In doing so, we build upon the work presented in Tollerud et al. (2011), who used strict isolation criteria to explore satellite galaxy counts around galaxies in the field. By focusing on isolated hosts, we are able to eliminate the known effects of massive haloes (groups or clusters) and large-scale structure on satellites. We further split the samples based on the star forming activity of the host to investigate the origins and strength of correlations between star formation properties of satellites and hosts (i.e. the physical drivers of galactic conformity). In Section 2, we introduce our observational sample, use N-body simulations to develop criteria for selecting isolated  $L^*$  hosts, and quantify the expected level of interloper contamination. In Section 3, we describe the selection criteria as applied to the SDSS to create our galaxy samples. In Section 4, we present our findings on the relationship between star formation properties of satellites and their host galaxies. Finally, we discuss and summarize the implications of the observed trends on galaxy formation models in Section 5 and Section 6. Unless otherwise noted, all logarithms are base 10. Halo virial masses are defined with respect to an overdensity of 94 relative to the critical density of the universe (Bryan & Norman 1998). Throughout our analysis, we employ a  $\Lambda$  cold dark matter ( $\Lambda$ CDM) cosmology with WMAP7+BAO+H0 parameters  $\Omega_\Lambda = 0.73$ ,  $\Omega_m = 0.27$ , and  $h = 0.70$  (Komatsu et al. 2011).

## 2 USING SIMULATIONS TO DEFINE THE OBSERVATIONAL SAMPLE

Before we detail our approach to isolate host galaxies and their satellites, a brief description of our adopted terminology is in order.

We use the term “satellite” to refer to a galaxy that is within the virial volume of a central “host” galaxy’s halo. Given that the observational data are subject to projection effects, we refer to our raw sample of observed galaxy pairs as “primaries” and “secondaries”. We also construct theoret-

ical mock catalogs, and use the terms host and satellite once the full three-dimensional information in the simulation is used to confirm whether an “observed” secondary is actually within the virial volume of the primary. Finally, based on these mock observations, our observationally-derived statistics will be corrected for contamination effects; accordingly, we will use the terms “host” and “satellite” in discussing contamination-corrected observed parameter distributions as well.

### 2.1 Observational Data

In selecting our observational sample, we employ data from Data Release 7 (DR7) of the Sloan Digital Sky Survey (SDSS York et al. 2000; Abazajian et al. 2009). In particular, we utilize the MPA-JHU derived data products, including median total stellar masses, photometrically derived according to Kauffmann et al. (2003, see also Salim et al. 2007), and median total star formation rates, measured from the SDSS spectra as detailed by Brinchmann et al. (2004). Note that their procedure includes methods for estimating specific star formation rates when they are unobtainable from emission lines. Supplemental information is drawn from the NYU Value-Added Galaxy Catalog (NYU-VAGC Blanton et al. 2005b), such as Sérsic indices (Sérsic 1968) that are derived from one-component fits according to Blanton et al. (2003, 2005a).

As a first step in identifying satellite and host galaxies, we compile a list of secondaries containing all galaxies with a stellar mass of  $10^{9.5}M_\odot < M_\star < 10^{10.5}M_\odot$  and a list of primaries with  $M_\star > 10^{10.5}M_\odot$ . As discussed in more detail in Section 2.3, we then apply isolation criteria to the potential primary sample and spectroscopically search for physically-associated secondaries. We also impose a spectroscopic completeness (*fgotmain*) cut of 0.7. This cut corresponds to a mean sample spectroscopic completeness of 92%, making it extremely unlikely that an object for which no redshift was obtained would impact our isolation procedure. Furthermore, we do not expect the small remaining incompleteness to bias our satellite selection. Our final samples of primary and secondary galaxies have mean stellar masses of  $M_\star = 10^{10.80}M_\odot$  and  $M_\star = 10^{9.97}M_\odot$ , respectively. We impose a limiting redshift of  $z = 0.032$ , within which we are complete to a stellar mass of  $10^{9.5} M_\odot$ . The mean redshift of our sample is 0.027. Our final sample contains 457 primary/secondary systems. These parameters are similar to the selection criteria described in Tollerud et al. (2011).

We further divide the primaries into active and passive categories, with the dividing line between the the two star formation rate classes given by

$$\log(\text{SSFR}_{\text{host}}) = -0.6 \log(M_{\star, \text{host}}) - 5.2, \quad (1)$$

where  $\text{SSFR}_{\text{host}}$  denotes the specific star formation rate of the host galaxy. This equation is motivated by the established blue cloud/red sequence dichotomy of galaxies in the SDSS (Strateva et al. 2001; Baldry et al. 2004; Blanton et al. 2005a). The slope was selected to match the slope of the red sequence in our sample.

## 2.2 Numerical Simulation

Our goal of studying satellites of isolated  $L^*$  galaxies requires a rigorous and accurate identification of truly isolated  $L^*$  primaries, systems that are largely excluded from residing within group and cluster environments. Accordingly, we use the Millennium-II Simulation (hereafter, MS-II; Boylan-Kolchin et al. 2009) to test our selection and isolation procedures. The MS-II has a box size of 137 Mpc, well-matched to our observational volume at  $z < 0.032$ . Its high mass resolution –  $m_p = 9.4 \times 10^6 M_\odot$  – ensures that it is complete for halo masses in excess of  $\sim 2 \times 10^{10} M_\odot$ , corresponding to stellar masses of  $\sim 10^{7.5-7.75} M_\odot$  (Guo et al. 2010; Behroozi, Conroy & Wechsler 2010; Behroozi, Wechsler & Conroy 2012; Leauthaud et al. 2012; Moster, Naab & White 2013). Using the MS-II, Tollerud et al. (2011) demonstrate the effectiveness of this technique in obtaining clean samples of isolated hosts with halo masses of roughly a few  $\times 10^{12} M_\odot$ .

Following the abundance matching prescription of Guo et al. (2010), we find that our lower limit for the stellar mass of secondaries ( $M_* = 10^{9.5} M_\odot$ ) corresponds to  $v_{\max} = 94.8 \text{ km s}^{-1}$ . The cutoff between what we consider to be a primary and a secondary,  $v_{\max, \text{cut}}$ , corresponds to a value of  $v_{\max, \text{cut}} = 166.5 \text{ km s}^{-1}$ . We use these values to construct mock catalogs below.

## 2.3 Obtaining Isolated $L^*$ Galaxies

Figure 1 illustrates the difficulty in selecting satellite galaxies around isolated  $L^*$  host haloes without significant contamination by cluster or group members. We use the MS-II simulation to perform a series of mock observations to identify secondaries and then determine the host virial mass of the associated subhaloes (horizontal axis) for various selection criteria. The black solid histogram shows the host halo virial mass distribution for all secondaries within a projected distance of  $d_{\text{proj}} = 355 \text{ kpc}$  of an identified primary. We count one host halo for each secondary identified, implying that that same host halo can appear more than once if it hosts multiple secondary candidates. It is evident that this selection picks out a large percentage of satellites that reside within group and cluster-mass haloes ( $M_{\text{vir}} > 10^{13} M_\odot$ ).

A standard additional criterion for spectroscopic secondary selection is a cut on the velocity difference between the primary and secondary,  $\Delta v$ . As we might expect satellites of group sized haloes to be kinematically warm, this cut could prove useful for excluding such massive hosts. However, restricting pairs to lie within a projected velocity limit  $\Delta v_{\text{sel}} = 500 \text{ km s}^{-1}$  only weakly eliminates haloes within the cluster and group mass regime (blue dashed histogram), while preferentially removing galaxy-sized ( $< 10^{12.5} M_\odot$ ) haloes (see blue dashed histogram in Fig. 1). Such a cut on velocity difference is ineffective at removing higher-mass haloes since group environments contain many objects – with a wide range of velocities – in the secondary range. As such, it is very likely that one of these objects will meet both our projected distance and projected velocity criteria, even if many or even most will not.

In order to filter out satellites associated with massive host haloes, we adopt an approach pioneered by Barton et al. (2007), which relies on strict isolation cuts (see also

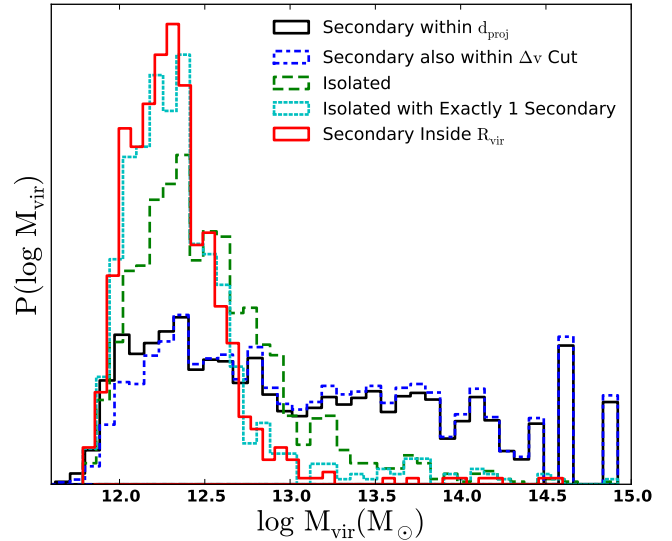


**Figure 1.** Probability distribution of virial masses of primaries associated with each secondary within a projected distance of  $d_{\text{proj}} = 355 \text{ kpc}$  for various selection cuts in the MS-II mock catalogs. Using only this  $d_{\text{proj}}$  criterion (black solid line), many of the selected secondaries are associated with very massive dark matter host primaries. Adding a restriction of  $\Delta v_{\text{sel}} = 500 \text{ km s}^{-1}$  does not help in isolating MW-size hosts, as cluster and group haloes typically contain galaxy pairs that satisfy this criterion. Further restricting this subset of primaries to those that are isolated (according to our fiducial set of isolation criteria as defined in Section 2.4) *significantly* reduces the high-mass tail (green dashed line). Adding the constraint that primaries have *exactly* one secondary (cyan dotted line) further decreases the number of group-mass ( $\sim 10^{13} M_\odot$ ) haloes selected. This line represents the halo mass distribution for our full sample. The red line demonstrates that in most group-scale systems in our sample, the secondary is outside the virial radius of the group’s central halo. Thus, even for the small number of group-sized haloes in our sample ( $< 7\%$  of secondaries), we do not expect physical mechanisms specific to the group environment to significantly bias our results.

Tollerud et al. 2011; Edman, Barton & Bullock 2012). Specifically, we impose limitations on  $n_{\text{iso}}$ , the maximum number of other haloes (galaxies) in the primary  $v_{\max}$  ( $M_*$ ) range that we allow within an annulus bounded on the interior by  $d_{\text{sel}}$  and on the exterior by  $d_{\text{iso}}$ , and bounded in velocity space by  $\pm \Delta v_{\text{iso}}$ . We never allow any other primaries within  $d_{\text{sel}}$  in projected distance space and  $\pm \Delta v_{\text{iso}}$  in velocity space. The green dashed histogram in Figure 1 shows the host halo mass distribution when we restrict our selection to only those haloes that (1) have no other primaries within  $d_{\text{sel}} = 355 \text{ kpc}$  and  $\Delta v_{\text{iso}} = 1000 \text{ km s}^{-1}$  and (2) have no more than one other primary within  $d_{\text{iso}} = 1 \text{ Mpc}$  and  $\Delta v_{\text{iso}} = 1000 \text{ km s}^{-1}$ . We will show below that this particular set of criteria are optimal for isolating MW-sized haloes and their LMC-sized companions, and also for maximizing the purity of our pair sample. With the isolation criteria imposed, we greatly reduce the number of haloes in our sample that inhabit clusters and somewhat reduce those in the group mass regime as well.

As a final cut, we select only those haloes that have *exactly* one secondary within 355 kpc and  $|\Delta v| < 500, \text{ km s}^{-1}$ . Applying this additional selection criterion (see the cyan

dotted histogram in Fig. 1) removes nearly all pairs that fall within groups and cluster, yielding a population dominated by Milky Way-like haloes; only 6.7% of objects satisfying our isolation and satellite number cuts occupy haloes with  $M_{\text{vir}} > 10^{13} M_{\odot}$  within the MS-II. Moreover, for the small tail of secondaries associated with massive primaries, only 38% of them actually lie inside the virial radius of the identified primary – the rest sit at the outskirts of their associated friends-of-friends group in the MS-II catalog. The red solid histogram in Figure 1 shows the mass distribution for secondary hosts that lie within the virial radius of their respective host haloes. The resultant histogram clearly picks out the galaxy-mass scale for hosts. The median host mass for this distribution is  $M_{\text{vir}} = 10^{12.29} M_{\odot}$  with a 68% spread of  $10^{12.17} - 10^{12.40} M_{\odot}$ . While it would be impossible to employ this in our observational sample, we do not expect satellites that lie outside of their host’s virial radius to contribute significantly to a quenching signal (Wetzell et al. 2013b).

The selection cuts illustrated by the cyan histogram in Figure 1 represent our fiducial choices for five parameters that we have tuned to identify exclusively bright satellites around isolated  $\sim L^*$  hosts. These choices are based on tests against mock observations in the MS-II simulation:

- $d_{\text{sel}} = 355$  kpc: The maximum projected separation between primary and secondary.
- $d_{\text{iso}} = 1$  Mpc: The maximum projected distance within which we check for neighbouring primaries.
- $n_{\text{iso}} = 1$ : The maximum number of neighbouring primaries allowed between  $d_{\text{proj}}$  and  $d_{\text{iso}}$  within  $\Delta v_{\text{iso}}$  in velocity. We always require that no neighbouring primary can fall within  $d_{\text{sel}}$  in projected distance and  $\Delta v_{\text{iso}}$  in velocity, such that the primary in our sample have no other primary within a distance of  $d_{\text{sel}}$ .
- $\Delta v_{\text{sel}} = 500 \text{ km s}^{-1}$ : The maximum line-of-sight velocity difference between primary and secondary.
- $\Delta v_{\text{iso}} = 1000 \text{ km s}^{-1}$ : The minimum line-of-sight velocity difference required between the primary and any other neighbouring primary within a projected distance of  $d_{\text{iso}}$  to not count towards  $n_{\text{iso}}$ . No neighbouring primary is allowed within  $d_{\text{sel}}$  and  $\Delta v_{\text{iso}}$ .

In the next subsection we illustrate how these fiducial choices were motivated to balance purity and sample size.

## 2.4 Balancing Purity and Sample Size

A crucial characteristic of any observational sample is its purity,  $f_{\text{purity}}$ , which we define within the MS-II to be the fraction of identified host-satellite pairs having (1) primaries that are actually host haloes (i.e. not satellites of a larger system); (2) secondaries that are actually satellites (i.e. not lower-mass primaries); and (3) satellites that are actually satellites of the host (and not satellites of a different host that are included because of projection). All of the parameters listed in Section 2.3 could be tuned to increase the purity of the sample, however this usually involves a trade-off with regard to sample size. As an illustration, we present one such example of this tuning: Figure 2 illustrates the dependence of sample purity on our isolation criterion,  $n_{\text{iso}}$ , holding all other parameters fixed at their fiducial values. As expected, increasing  $n_{\text{iso}}$  increases the number of interlopers and decreases  $f_{\text{purity}}$  (solid red line). While the purity of

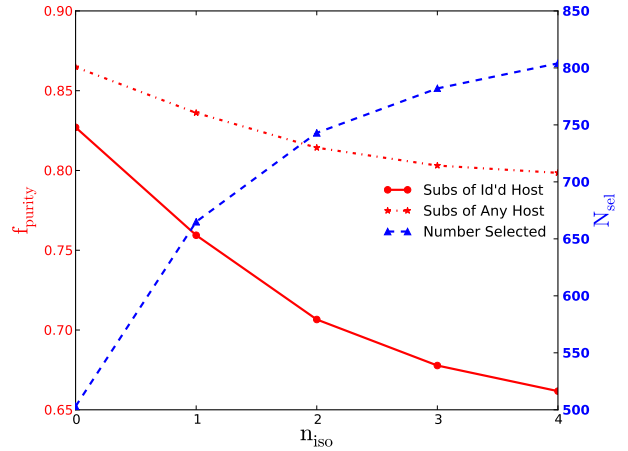


**Figure 2.** Fraction of the pair sample (in the MS-II) for which the secondary is a subhalo of the primary (red solid line) and for which the secondary is a subhalo of any host (red dash-dotted line) alongside the number of pairs selected (blue dashed line) as a function of one of our isolation criteria,  $n_{\text{iso}}$ . While purity rises sharply as  $n_{\text{iso}}$  approaches 0, the number of pairs selected decreases precipitously. As a compromise between sample size and purity, we define our selection limit to be  $n_{\text{iso}} = 1$ . At this value of  $n_{\text{iso}}$ , the secondary is a subhalo of the primary in 75% of pairs while the secondary is a subhalo of any host in just over 85% of the sample.

our sample increases with the strictness of our isolation criterion,  $n_{\text{iso}}$ , the sample size simultaneously decreases (blue dashed line). As a compromise between sample size and purity, we define our selection limit to be  $n_{\text{iso}} \leq 1$  throughout the remainder of this work, yielding a sample purity of 75%. While using  $n_{\text{iso}} = 0$  would increase the purity to 82%, it would also reduce the sample size by more than 25%.

Note that if we relax the definition of a true pair to require only that the secondary be a subhalo, rather than being a subhalo of the chosen host, our purity reaches approximately 85% and depends little on  $n_{\text{iso}}$  (dotted red line). In subsequent sections, we perform corrections to account for the presence of interlopers in the observational data using this modified definition of purity. We make the assumption that the interloper population is comprised only of field galaxies having the same specific star formation rate distribution as the control sample (see Section 4).

Purity could also vary within our sample as a function of separation between the primary and secondary galaxy, either in physical space or velocity space. While sample size and purity exhibit little dependence on  $\Delta v$ , we find significant variation in purity with the projected separation between the primary and secondary. As shown in Figure 3, sample purity increases with decreasing  $d_{\text{proj}}$  for both our standard and less-restrictive definition of purity (blue solid and red dashed lines, respectively). For close separations ( $\sim 60$  kpc), approximately 88% of secondaries are subhaloes of their respective primaries. At larger distances, however, the problem of contamination increases noticeably. At  $\sim 200$  kpc, the purity drops to  $\sim 77\%$ , while it falls to just over 50% at 300 kpc. Even when considering whether the secondary is a subhalo of any host, the purity decreases from  $\sim 96\%$  in the innermost bin to 86% at 200 kpc and 70% at 300 kpc. When

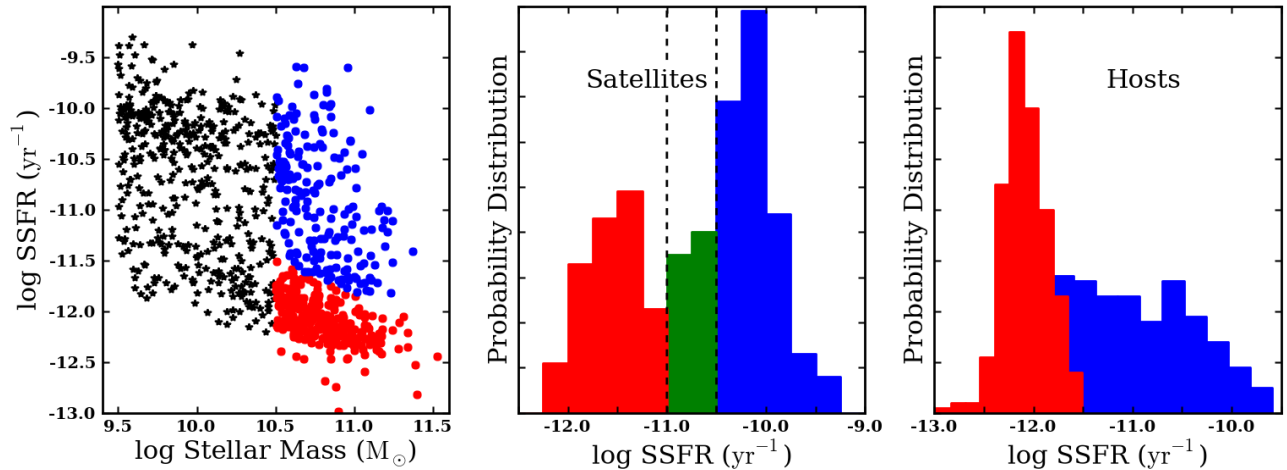


**Figure 4.** (*Left*): The distribution of specific star formation rate (SSFR) as a function of stellar mass for the galaxy sample employed in this study. Galaxies with  $M_* > 10^{10.5} M_\odot$  are categorized as hosts (red and blue points), with galaxies at lower mass categorized as satellites (black stars). Hosts are divided into two samples, where those coloured blue are star forming and those coloured red are passive. Each host has exactly one satellite. (*Centre*): The SSFR distribution for the satellite population. For the purposes of quantifying quenching effects, we subdivide the satellite population into three categories of star formation activity: satellites with SSFRs greater than  $10^{-10.5} \text{ yr}^{-1}$  are defined as vigorously star forming (blue histogram), satellites with SSFRs between  $10^{-10.5} \text{ yr}^{-1}$  and  $10^{-11} \text{ yr}^{-1}$  are defined as moderately star forming (green histogram), and satellites with SSFRs less than  $10^{-11} \text{ yr}^{-1}$  are deemed passive (red histogram). (*Right*): Distribution of SSFRs for host galaxies. Hosts are divided into passive (red histogram) and star forming (blue histogram) subsamples according to blue cloud/red sequence membership as detailed in Equation 1.

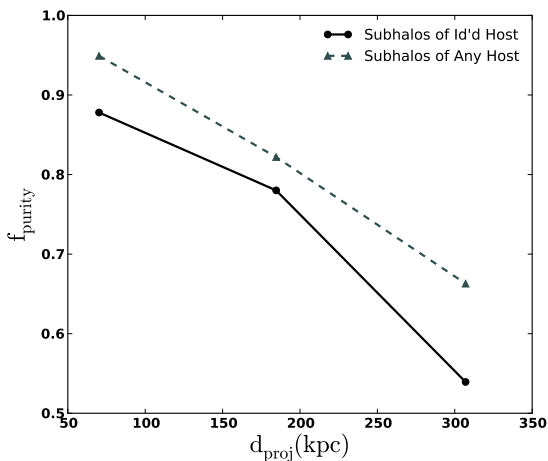


**Figure 3.** Fraction of the pair sample for which the secondary is a subhalo of the primary (solid line) and for which the secondary is a subhalo of any host (dashed line) as a function of projected distance between the primary and secondary in the MS-II. Due to an increased chance of interlopers at larger  $d_{\text{proj}}$ , the purity decreases with projected distance from the primary. The fraction of secondaries that are true subhaloes of the primary decreases from  $\sim 88\%$  in the innermost bin to just above 50% at 355 kpc, while the fraction of secondaries that are subhaloes of any host decreases from  $\sim 96\%$  in the innermost bin to 70% at 355 kpc.

we consider trends in quenching with projected radius, we will take this radial dependence on purity into consideration.

### 3 ISOLATED $L^*$ HOSTS IN SDSS

#### 3.1 Isolation Procedure Applied to Data

Having identified an optimal set of selection criteria, we turn to applying these criteria to our observational data. To identify a set of potential primary galaxies, we begin by selecting all galaxies in the SDSS DR7 catalog with stellar mass greater than  $10^{10.5} M_\odot$ . The isolation criteria described in Section 2.3 are then applied. In particular, we discard (1) all primaries with one (or more) neighbour of stellar mass  $M_* > 10^{10.5} M_\odot$  within a projected distance of 355 kpc and within a velocity difference of  $|\Delta v| \equiv c|z_1 - z_2| < 1000 \text{ km s}^{-1}$  along the line-of-sight, and (2) all primaries with two (or more) neighbours of stellar mass  $10^{10.5} M_\odot$  having  $355 \text{ kpc} < d_{\text{proj}} < 1 \text{ Mpc}$  and  $|\Delta v| < 1000 \text{ km s}^{-1}$ . All galaxies that pass the isolation criteria are deemed “isolated host-mass primaries.” We then compile a catalog of host/satellite pairs, our “pairs catalog,” by selecting those isolated host mass primaries with exactly one neighbour in the stellar mass range  $10^{9.5} M_\odot < M_* < 10^{10.5} M_\odot$  with  $d_{\text{proj}} < 355 \text{ kpc}$  and  $|\Delta v| < 500 \text{ km s}^{-1}$ . As shown in the previous section, the requirement of exactly one satellite allows us to better select hosts that have MW-sized haloes (i.e.  $M_* \sim 10^{12} M_\odot$ ). After the full isolation procedure, our pairs catalog consists of 483 host-satellite partners. Based on the results of Section 2.3, we expect that the hosts have a median virial mass of  $1.9 \times 10^{12} M_\odot$ .

#### 3.2 Observational Sample

The left panel of Figure 4 shows our hosts and satellites in the specific star formation rate-stellar mass plane. Black stars denote the satellite population, while our host population is coloured by star formation properties (see Eqn. 1):

red and blue circles correspond to the passive and star forming hosts, respectively. Hosts with multiple bright satellites and satellites near two host-like objects were removed from the sample, such that there is a one-to-one correspondence between the hosts and satellites in the pairs sample.

The distribution of specific star formation rates for the satellite population is given in the central panel of Figure 4. We place vertical lines at  $10^{-11} \text{ yr}^{-1}$  and  $10^{-10.5} \text{ yr}^{-1}$  in this and all subsequent plots as the borders of our defined regimes of star formation activity for the satellite population: passive (red histogram), moderately star forming (green histogram), and vigorously star forming (blue histogram). Finally, the SSFR distribution for the hosts is shown in the right panel of Figure 4. Hosts are divided into passive and star forming categories according to Equation 1.

### 3.3 Satellite-host velocity distributions

In Figure 5, we show the distributions of  $\Delta v$  for our full primary/secondary sample (dash-dotted grey) along with those for our star forming primary sample (blue curve) and a stellar mass-matched subsample of our passive primaries (red curve). These histograms represent “stacked” satellite velocity distributions for hosts. By bootstrapping our distributions, we find evidence (at approximately two standard deviations) that passive hosts reside in slightly more massive haloes *at fixed stellar mass*, with measured velocity dispersions  $\sigma_{\text{passive}} = 165.1 \pm 8.3 \text{ km/s}$  and  $\sigma_{\text{starforming}} = 145.4 \pm 9.4 \text{ km/s}$ . This suggests that the haloes of passive  $L^*$  galaxies are  $\sim 45\%$  more massive at fixed stellar mass than those of star forming galaxies, assuming a mass-scaling proportional to  $\sigma^3$ , where the exponent is derived from the assumption of a linear relation between halo maximum circular velocity and the spread of stacked pairwise host/satellite velocity distributions at fixed halo mass.<sup>1</sup> Also plotted is the distribution of velocity differences for the objects in MS-II chosen by mock observations that mirror our selection criteria (black histogram). Remarkably, the mock catalog falls almost perfectly between the red and blue histograms, providing an independent dynamical verification that we are indeed selecting the haloes we have set out to study using abundance matching.

The evidence we see for a halo mass trend with SSFR at fixed stellar mass is qualitatively consistent with the results of Mandelbaum et al. (2006), who find that early-type galaxies with stellar masses of  $\sim 10^{11} M_{\odot}$  tend to live in haloes that are  $\sim 3$  times more massive than their star forming counterparts at the same stellar mass. The Mandelbaum et al. (2006) work samples all environments and thus the mass trend may be a result of the colour-density relation where red galaxies prefer overdense regions – i.e. more massive haloes (Hogg et al. 2004; Cooper et al. 2006, 2010a,b).

<sup>1</sup> The qualitative result that passive hosts reside in kinematically warmer and thus more massive haloes is robust to the exact nature of the scaling between stacked satellite velocities and halo mass. We have used simulated observations described in Section 2.2 to compare the observed velocity dispersions of satellite subhalos within hosts stacked in virial mass bins and found that the naive scaling adopted here does hold for the halo mass range of interest.

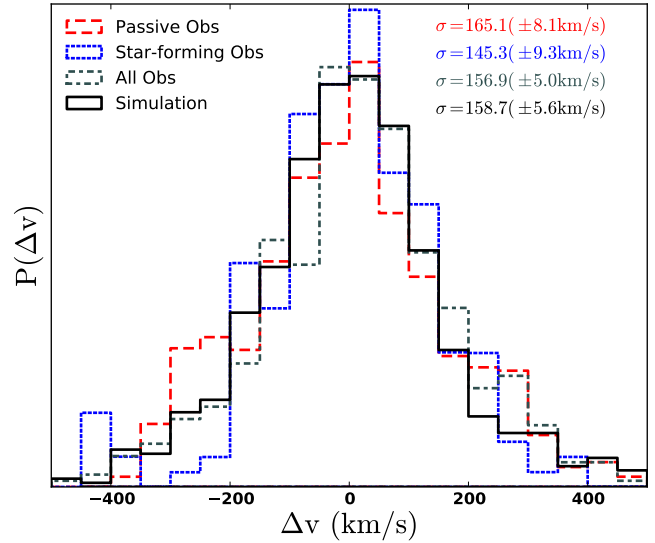


**Figure 5.** Probability distribution of velocity offsets  $\Delta v$  for all observed primary-secondary pairs in our sample (dash-dotted grey) along with pairs chosen from stellar mass-matched samples of star forming (blue) and passive (red) hosts. The root-mean-square of each distribution is given in the figure. The passive host subsample appears kinematically warmer than the star forming host subsample, suggesting that these passive galaxies reside in more massive dark matter haloes at fixed stellar mass. Also shown are the host-satellite velocity distributions for our mock catalogs with the same selection criteria applied to MS-II (black line), which matches well the observed sample. This remarkable consistency shows that our selection procedure is identifying host haloes as expected, with a virial mass distribution consistent with that shown by the red histogram in Figure 1.

Our sample focuses on lower-mass systems, and specifically avoids group and cluster haloes.

### 3.4 Control Sample

As a reference sample by which to compare our satellite population, we define a set of galaxies in the field with stellar masses similar to that of our satellite galaxies. As with our pairs sample, we tune our selection criteria by maximizing purity, where purity here is defined to be the fraction of objects that are actually hosts (i.e. centrals) and not satellites within the MS-II. Since we have no shortage of objects (SDSS contains 12447 such objects in our stellar mass range), conserving sample size is less important, and we can tune our selection parameters to create a maximally pure control sample. The final selection parameters for the control sample are  $n_{\text{iso,control}} = 0$ ,  $d_{\text{iso,control}} = 2.9 \text{ Mpc}$  and  $\Delta v_{\text{iso,control}} < 400 \text{ km s}^{-1}$ . With these values for the selection and isolation criteria, we obtain  $f_{\text{p,control}} = 0.97$ . The impurity in the sample is approximately equal to the Poisson noise from the number of objects,  $1 - f_{\text{purity,control}} = 1/\sqrt{N}$ .

Implementing these selection criteria, we construct a catalog of isolated galaxies in the mass range  $10^{9.5} < M_{\star} < 10^{10.5}$  to use as our control sample. Our isolation criteria are similar to, but more stringent than, those used in selecting the pairs catalog. We reject any galaxy with a neighbour of stellar mass  $\log(M_{\star}/M_{\odot}) > 9.5$  with  $d_{\text{proj}} < 2.9 \text{ Mpc}$  and with  $\Delta v_{\text{iso}} < 400 \text{ km s}^{-1}$ . This catalog, which we will call

the “field dwarf catalog” contains 581 galaxies, with a mean stellar mass of  $10^{9.95} M_{\odot}$  and a mean redshift of 0.024.

### 3.5 Parameter-Matching Procedure

It will frequently be useful in our analysis to explore the variation in a given galaxy property (e.g. specific star formation rate) across two related samples of galaxies (e.g. isolated galaxies versus satellites). When performing such a comparison, we would like to control for correlations between the varied parameter and other properties of the chosen samples — for example, the observed decrease in SSFR with increasing stellar mass (Brinchmann et al. 2004; Noeske et al. 2007; Elbaz et al. 2007). To do so, we match the stellar mass distribution of a subsample of the field dwarf catalog to the subsample of satellite galaxies under study; this ensures that the two samples have statistically identical distributions of stellar mass. We divide both samples into bins (typically 10, although we allow this to vary based on sample size) in the relevant parameter, then randomly select galaxies with replacement from the sample with the larger number in that bin, until both subsamples have an equal number in the bin. This procedure is repeated 100 times, and the results given below are mean values.

## 4 SATELLITE QUENCHING AS A FUNCTION OF CENTRAL GALAXY PROPERTIES

The primary goal of this paper is to explore the degree to which satellite galaxies have suppressed or quenched star formation relative to similar galaxies in the field. In order to numerically interpret our results, we introduce a conversion fraction ( $f_{\text{convert}}^X$ ), designed to indicate the fraction of galaxies that are converted from star forming to suppressed/quenched *because* they are satellites.

Mathematically, the conversion fraction is defined as follows. Let  $X = \log(\text{SSFR})$  indicate a variable value for the specific star formation rate. Define the unquenched fraction (with  $\log \text{SSFR} \geq X$ ) of satellites and control galaxies to be  $u_{\text{sat}}$  and  $u_{\text{control}}$ , respectively. The associated quenched fractions with  $\log \text{SSFR} < X$  are  $q_{\{\text{sat}, \text{control}\}} = 1 - u_{\{\text{sat}, \text{control}\}}$ . The conversion fraction,  $f_{\text{convert}}^X$ , is then given by

$$f_{\text{convert}}^X = \frac{q_{\text{sat}} - q_{\text{control}}}{u_{\text{control}}} \Bigg|_{\text{SSFR}=10^X}. \quad (2)$$

For example, if 100% of the galaxies in the control sample are star forming (at the given SSFR threshold) but only 80% of the satellite galaxies are star forming (at the same threshold), then  $f_{\text{convert}} = 0.2$  and we may conceivably argue that  $\sim 20\%$  of star forming galaxies were converted to quenched galaxies after becoming satellites. Likewise, for star forming fractions of 60% and 40% for the control and satellite samples (respectively), the conversion fraction would be  $f_{\text{convert}} = 0.33$ .

This definition of conversion fraction is similar to the similar quenching efficiency specified by e.g. van den Bosch et al. (2008); Peng et al. (2012), although  $f_{\text{convert}}^X$  is generalized to be a function of SSFR. The two conversion fractions we will primarily consider are  $X = -11$  and  $X = -10.5$ . The conversion fraction evaluated at the passive SSFR threshold

for satellites,  $f_{\text{convert}}^{-11}$ , can be thought of as the fraction of satellites that were star forming prior to infall and have subsequently been converted to passive satellite systems, making it an effective method of quantifying quenching. The conversion fraction evaluated at the border between vigorous and moderate star formation,  $f_{\text{convert}}^{-10.5}$ , is representative of the fraction of vigorous star forming galaxies that upon infall had their star formation either reduced to a moderate level or halted entirely. In general, we will refer to a satellite’s SSFR being lowered below  $10^{-11} \text{ yr}^{-1}$  as “quenching,” and the general case of a satellite’s SSFR being lowered as “suppression” (e.g. we will often discuss  $f_{\text{convert}}^{-10.5}$  as suppression of vigorous star forming satellites). We will make use of these parameters throughout the remainder of this work.

### 4.1 All Satellites

Figure 6 shows the cumulative distributions of SSFRs for all satellite galaxies in our sample. The dashed red line is the observed distribution SSFR for the satellite population, while the solid red line is the corrected satellite distribution, where the observed distribution is adjusted to take into account the presence of interlopers. This is done by subtracting the control distribution scaled by the probability that a randomly selected galaxy is an interloper,  $(1 - f_{\text{purity}})$ , from the satellite distribution. The adjusted distribution is then re-normalized.<sup>2</sup> This correction for purity is made in each plot of satellite SSFR that follows, and the uncorrected result is omitted. The black line shows the distribution for the mass-matched field control sample — i.e. for a sample of isolated (central) galaxies with the same stellar mass distribution as the satellites. For both the corrected satellite and control samples, binomial errors are shown by the corresponding shaded region according to the formula

$$\sigma^2 = \frac{(q_{\text{sample}})(u_{\text{sample}})}{N_{\text{sample}}} \quad (3)$$

where  $q_{\text{sample}}$  is the sample’s quenched fraction,  $u_{\text{sample}}$  is the sample’s unquenched fraction, and  $N_{\text{sample}}$  is the total number of objects in the sample.

Globally,  $f_{\text{convert}}^{-11} = 0.18$  for our  $L^*$  host sample, with a similar value for  $f_{\text{convert}}^{-10.5}$ . This implies that approximately 20% of satellites are quenched as a result of falling into their host’s virial radius. The right panel of Figure 6 generalizes  $f_{\text{convert}}$  to an arbitrary SSFR threshold. Bright satellite galaxies residing in haloes similar to that of the Milky Way show an overall flat increase in conversion fraction over a dex in satellite SSFR ranges. We use this style of presentation in the next three plots; the left panels show the cumulative distributions of SSFR for the satellite and control samples and the rightmost panel shows  $f_{\text{convert}}$  plotted as a function of satellite threshold SSFR (as defined by Equation 3).

### 4.2 Dependence on Host Star Formation Rate

In order to investigate the correlation of quenching efficiency with host star formation activity, we define a mass-dependent passive threshold according to SSFR in our host

<sup>2</sup> This assumes that the interlopers follow the same specific star formation distribution as the control sample.

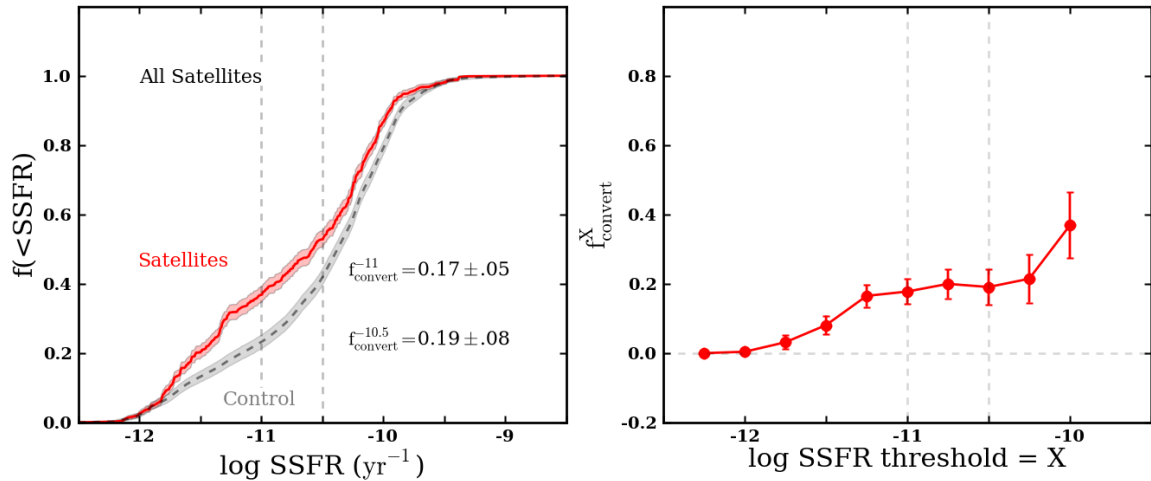


**Figure 6.** (*Left*): Cumulative distributions of specific star formation rate for the observed satellite sample (red dashed line), the purity-corrected satellite sample (red solid line), and the control sample (black dashed line). After a modest statistical correction for interloper contamination, we find that  $L^*$  hosts quench  $\sim 20\%$  of their infalling star forming satellites. Black and red shaded regions correspond to  $1\sigma$  binomial errors for the control and purity-corrected satellite samples, respectively. (*Right*): Conversion fraction as a function of specific star formation threshold  $X$ , which provides an estimate for the fraction of satellites that have had their star formation suppressed below a threshold value  $X$  as a result of becoming satellites. This quantity is defined in equation 3. The conversion fraction,  $f_{\text{convert}}$ , is quite flat over a wide range in satellite star formation rates. Vertical dashed lines correspond to our definitions of “quenched” and “vigorously star forming” satellites.

sample, given as Equation 1 above. Hosts that fall below the relation are considered passive ( $N = 267$ ,  $\langle M_\star \rangle = 10^{10.81} M_\odot$ ), while those above it are considered star forming ( $N = 190$ ,  $\langle M_\star \rangle = 10^{10.78} M_\odot$ ). Our goal of determining the correlation between star formation activity in satellites and hosts is complicated by the fact that passive hosts tend to have slightly higher stellar masses. To avoid biasing our results, we mass-match the host samples — i.e. we ensure that the distribution of stellar masses is the same between our star forming and passive host samples.

Comparisons of the cumulative distributions of satellite SSFRs for the two mass-matched host samples are shown in Figure 7. The satellite population around quenched hosts (middle panel) is itself quenched relative to the mass-matched field sample, with  $f_{\text{convert}}^{-11} = 0.28$  and  $f_{\text{convert}}^{-10.5} = 0.35$ . This result is qualitatively consistent with the observed correlation between host and satellite properties otherwise known as “galactic conformity” (e.g. Weinmann et al. 2006; Kauffmann et al. 2013; Robotham et al. 2013).

Remarkably, the satellite population around star forming hosts (left panel) is markedly different, with a SSFR distribution that is *indistinguishable* from the mass-matched sample of field galaxies. The right panel of Figure 7 emphasizes this stark difference — at all choices of SSFR threshold, the conversion fraction for satellites of star forming hosts (blue line) is consistent with zero. Meanwhile, the conversion fraction for passive hosts increases monotonically as the SSFR threshold decreases, suggesting that passive hosts are more likely to suppress vigorous star formation in their satellites than strongly quench it to passivity.

Figure 7 provides a compelling demonstration that satellite quenching and central quenching are strongly related: among bright  $\sim 0.1L^*$  satellites, only those that inhabit quenched hosts are themselves quenched (relative to the field population). This is somewhat distinct from the

view usually discussed as galactic conformity, in which the colour or star formation rate of a satellite is correlated with the colour or star formation rate of its host. Rather, it appears that bright satellites of isolated, star forming  $L^*$  galaxies are essentially unaffected by their host, whereas approximately 25-35% of satellites of quenched hosts are quenched as a result of being a satellite. The implications of this finding will be discussed in Section 5.

### 4.3 Dependence on Satellite Morphology

The previous subsection demonstrated that the quenching of  $\sim 0.1L^*$  satellites only occurs around galaxy-size hosts that are themselves quenched. A natural extension of this result is to ask whether the morphologies of the satellites are affected along with their star formation rates, where in this work we will use Sérsic index as a proxy for morphology. In other words, is the quenching mechanism connected to a morphological change?

Figure 8 explores this question by comparing the Sérsic index distributions for passive and star forming satellites of quenched hosts to mass-matched control samples of the same star formation category (passive or star forming). Neither satellite sample shows substantial deviation from the field. One might expect to observe no morphological difference between the star forming satellite sample. However, it is less obvious why the passive field dwarf sample resembles the passive satellite sample when the field galaxies are manifestly not being quenched by an environmental process, and a substantial fraction of the passive satellites of passive galaxies are.

It is clear from Figure 8 that whatever is causing satellite galaxies to be quenched at a higher rate than field galaxies, this process results in morphological properties that are indistinguishable from field galaxies that are presumably

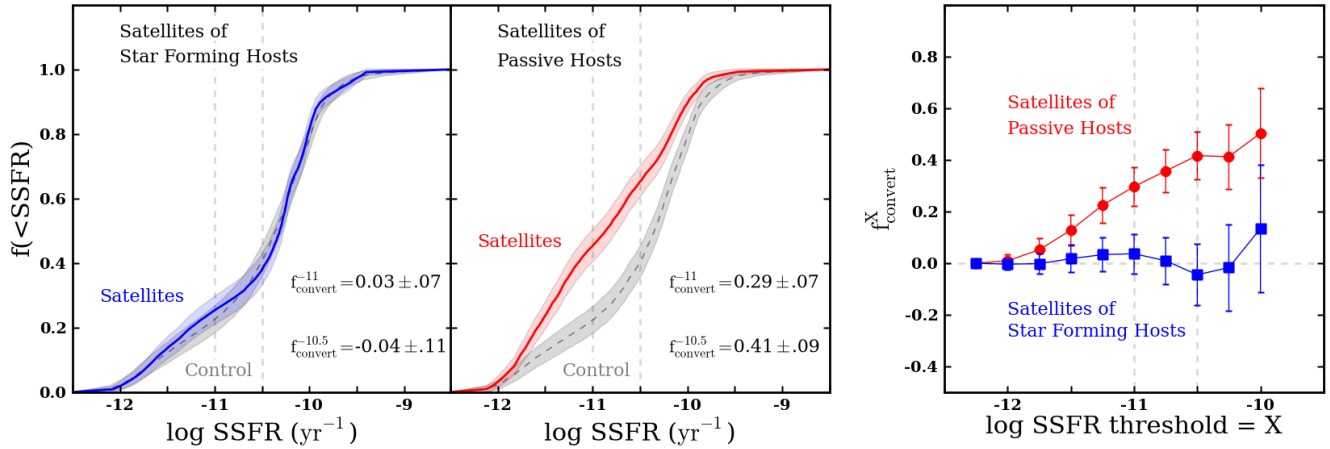


**Figure 7.** (*Left*): Cumulative distributions of specific star formation rate for satellites surrounding star forming hosts (blue line) and passive hosts (red line), with relevant mass-matched control samples (black dashed lines). Passive hosts quench  $\sim 30\%$  of their infalling star-forming satellites, while star forming hosts have satellite populations that very closely match the field. Shaded regions are binomial errors. (*Right*): Conversion fraction vs. threshold SSFR (see equation 3) for satellites of star forming and passive hosts. At all values of  $X$ , the satellites of star forming hosts are indistinguishable from the field population at the same stellar mass. In stark contrast, satellites of passive hosts show an increasing difference from the field at higher values of SSFR.

quenched via some distinct secular process. One potential implication is that the morphological differences that divide quenched and star forming galaxies are a *result* of a galaxy being quenched. This is distinct from the idea of “morphological quenching” that suggests that morphological changes themselves give rise to suppressed star formation (Martig et al. 2009). We return to a discussion of these issues in Section 5.

#### 4.4 Dependence on Projected Separation

We expect that the efficiency of some potential quenching processes may vary with the separation of the host and satellite, possibly reflecting radial variation in the circumgalactic medium (CGM) surrounding the host, the strength of the local tidal field, or the time since first infall for the satellite. In order to investigate trends with host/satellite distance, we place our satellite sample into three linearly spaced bins in projected separation. Conversion fractions are shown as a function of projected distance from the host, with samples divided according to SSFR in Figure 9. Sub-samples in each bin of projected separation are matched on host mass and compared to control samples matched to the corresponding satellite mass distributions. When examining the dependence of  $f_{\text{convert}}^{11}$  on satellite/host separation, we find a gradient in quenching efficiency. Around passive hosts, quenching persists only out to the intermediate projected radius bin, which has its outer edge at 236 kpc, less than the characteristic virial radius of our primary sample in MS-II ( $\sim 400$  kpc). Around star forming hosts, however, we find results consistent with no quenching at all radii.

The right panel of Figure 9 shows  $f_{\text{convert}}^{10.5}$ , which is sensitive to the *damping* of vigorous star formation, if not full quenching. The trends are highly similar in shape; the largest difference is the central value in the innermost bin of the star forming host sample. Again, we see no evidence of

quenching around star forming hosts, and strong quenching around passive hosts.

## 5 DISCUSSION

The main result from our study of central and satellite galaxies in the SDSS is that bright satellites of  $\sim L^*$  galaxies are only quenched beyond what is seen in the field around passive hosts, indicating a strong connection between the quenching of satellites and centrals in Milky Way-like haloes. This host-specific dichotomy in satellite quenching is likely (or at least partially) responsible for the observed correlation between the properties of central and satellite galaxies in the local Universe, a phenomenon commonly dubbed “galactic conformity.” As first shown by Weinmann et al. (2006), studying more massive haloes than those isolated in our work, groups dominated by a “late-type” central host a higher fraction of “late-type” satellites relative to groups populated by an “early-type” central.<sup>3</sup> More recently, results from Wang & White (2012) highlight a similar conformity in the rest-frame  $g - r$  colour of satellite galaxies in the SDSS, examining systems across a broad range of host stellar mass. Lastly, studying low-mass galaxy groups identified by the Galaxy And Mass Assembly project (GAMA, Driver et al. 2011), Robotham et al. (2013) find that conformity is also evident in the morphological properties of satellites relative to their hosts, such that bulge-dominated central galaxies tend to host bulge-dominated satellites in contrast to disk-dominated centrals. Previous works have demonstrated that semi-analytic models do show evidence of galactic conformity, however the nature of the conformity does not match observations. For example, Wang & White (2012) argue that

<sup>3</sup> Note that the terms late- and early-type as used by Weinmann et al. (2006) correspond to the colour and/or SSFR of the galaxy and do not refer to a morphological classification.

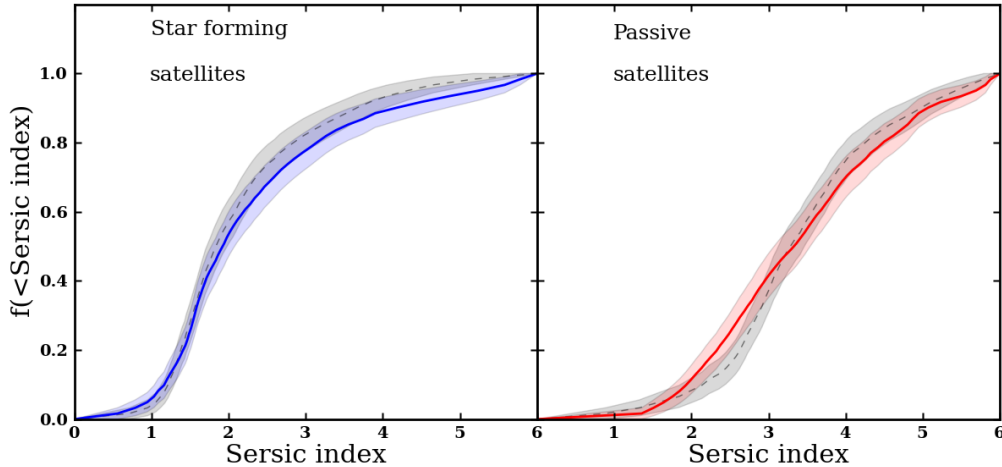


**Figure 8.** Cumulative distributions of Sérsic indexes for star forming (left panel) and passive (right panel) satellites around passive hosts and mass matched control samples (black dashed lines). Satellites show no significant difference in morphology relative to field galaxies at fixed stellar mass and star formation activity. Shaded regions are binomial errors.

the semi-analytic model of Guo et al. (2011) overpredicts the number of red satellites in g-r (colour). Similarly, we have analyzed the Guo et al. (2011) model results independently and found that they predict a conversion fraction of 0.6 around passive hosts and 0.3 around star-forming hosts, where we apply our same isolation criteria to the SAM. This is in stark disagreement with the dichotomy we see in the data.

In general, our results are in agreement with each of the aforementioned observational analyses. However, unlike these previous studies that compare the composition of  $\gtrsim 10^{12} M_{\odot}$  haloes separated according to the properties of the central galaxy (i.e. excluding the field population), our analysis extends this work to focus on the comparison of satellite samples (again divided according to the properties of the central) to field galaxies of like stellar mass. This is a critical step towards understanding the physical driver of satellite quenching in the local Universe, as it directly compares satellite galaxies to their parent population (i.e. field systems of like mass).

One possible explanation for the observed dichotomy in satellite quenching evident in our sample could be a dependence of quenching efficiency on halo mass. That is, passive hosts could live in more massive dark matter haloes relative to their star forming counterparts at fixed stellar mass, with quenching operating more efficiently in more massive haloes. As detailed in Section 3, we tailored our host selection criteria to isolate a sample that spans a relatively small spread in halo mass (FWHM  $\sim 0.5$  dex) and peaks at a few  $\times 10^{12} M_{\odot}$ . Studies of gas accretion onto dark matter haloes indicate that there is a transition in the dominant accretion mode at roughly this halo mass, with infalling gas shock-heated at the virial radius in haloes above a threshold mass of  $\sim$  a few  $\times 10^{12} M_{\odot}$ , while cold gas reaches a smaller radius, possibly falling all the way to the galaxy in less-massive haloes (e.g. Binney 1977; Rees & Ostriker 1977; Birnboim & Dekel 2003; Kereš et al. 2005, 2009; Stewart et al. 2011). Such a variation in accretion mode could manifest itself as a correlation between the star forming prop-

erties of central (and also satellite) galaxies and the mass of their host dark matter haloes, such that passive central galaxies reside in more massive dark matter haloes relative to star forming central galaxies of comparable stellar mass.

Recall that in our analysis, we tune our isolation criteria to identify haloes comparable in mass to that of the Milky Way, but select our sample of star forming and passive hosts for comparison by matching them in stellar mass (i.e. potentially allowing a weak correlation between halo mass and host properties). In Figure 5, we investigate this possibility by plotting separately the stacked velocity distribution of stellar mass-matched subsamples of satellites around our passive and star forming host galaxies. While we find that the red hosts are biased towards slightly more massive haloes (approximately 45% more massive), the difference is only significant at the  $\sim 1 - 2\sigma$  level. Furthermore, previous work examining galactic conformity by Weinmann et al. (2006) found that the correlation between the colour of central and satellite galaxies exists at fixed halo mass, looking at groups in the Yang et al. (2007) catalog, where the halo masses computed in the group catalog are based on the total luminosity or stellar mass of all member galaxies above a given luminosity threshold. This suggests that a potential dependence of quenching efficiency on halo mass is unable to explain our results in concert with those of Weinmann et al. (2006); while we find evidence for conformity at fixed *stellar* mass (and similar, though possibly not identical halo mass), Weinmann et al. (2006) claims conformity at fixed *halo* mass, although that result is consistent with ours.

The dichotomy in satellite quenching also could be driven by differences in the circumgalactic medium (CGM) of passive and star forming hosts. The CGM of the host halo could potentially affect the star formation of a satellite galaxy via two physical processes: (i) “ram pressure stripping,” where the cold interstellar gas from which stars could be actively formed is removed from the satellite, rapidly truncating its star formation (e.g. Gunn & Gott 1972; Bekki 2009) and (ii) “strangulation,” where the satellite retains its cold gas, allowing active star formation, but loses its reser-

voir of warm gas that would otherwise replenish the cold gas as it is exhausted (e.g. Larson, Tinsley & Caldwell 1980; Kawata & Mulchaey 2008). In either scenario, our results could be explained by the presence of a hot gaseous corona preferentially surrounding passive hosts, such that it prevents the infall of cold gas onto the central galaxy, thereby quenching it, while similarly halting the star formation of associated satellites. A CGM dichotomy could also arise in association with the the transition between cold and hot mode accretion. While realistically we expect there to be some scatter in the halo mass scale where the transition occurs (Kereš et al. 2009), there might naturally be a correlation between star formation in the central galaxy and ongoing cold-mode accretion. In hot mode haloes, star formation may be naturally suppressed by a lack of fuel, and the associated build-up of a hot corona could then provide a CGM-related suppression mechanism.

In our discussion of the hot CGM interpretation, we must address the results of Tumlinson et al. (2011): quasar line-of-sight probes of the CGM of nearby systems show an enhancement in ionized oxygen around star forming galaxies relative to their quenched counterparts, indicating that star forming galaxies host more warm gas in their haloes. The lack of O VI around passive hosts could be explained as a temperature effect, with passive galaxies surrounded by a typically hotter CGM. Observations of X-ray coronae around local ellipticals support this conclusion (O’Sullivan, Forbes & Ponman 2001; Sun et al. 2007), including recent work to study the hot gas surrounding lower-mass, isolated ellipticals (Mulchaey & Jeltama 2010; Humphrey et al. 2011, 2012).

In Section 4.3, we also examined the morphology of the satellites in our sample, finding consistent Sérsic indices at fixed stellar mass between the quenched satellites and quenched galaxies in the field. The same is true for star forming satellites. This result could be compared to similar results in van den Bosch et al. (2008), who found consistent concentrations between satellites and centrals at fixed stellar mass and colour, and Bamford et al. (2009) who found no trend in the early-type fraction of galaxies with environment in the sparse regime (and a weak trend, as compared to the trend in red fraction, over all environments). The lack of any difference between satellite and field morphology could provide a clue to the origin of the well-established link between structure and star formation in galaxies (e.g. Kauffmann et al. 2003; Blanton et al. 2005a; Wuyts et al. 2011; Bell et al. 2012; Cheung et al. 2012), with quenched galaxies typically having more bulge-dominated morphologies than star forming ones.

One idea to explain the correlation between morphology and star formation activity posits that the morphological transformation itself is the driving agent. Specifically, in the “morphological quenching” scenario (Martig et al. 2009), the presence of a bulge component stabilizes a galaxy against fragmentation to bound clumps, thereby halting star formation. In such a picture, a bulge-dominated galaxy may remain quenched even if it accretes gas (i.e. regardless of the assumed halo mass-dependent accretion mode). Our results may be at odds with such a scenario: satellites that are apparently quenched via environmental mechanisms never experienced by quenched galaxies in the field nevertheless have exactly the same distribution of morphological indexes.

If morphology were really the driver of quenching, it seems unlikely that this would be the case, unless somehow the passive-halo environment causes exactly the same type of bulge formation as do processes in the field. One might argue that tidal forces could incite secular instabilities, but this would also produce quenching for satellites around non-star forming hosts. No such signal is seen.

Often, galaxy mergers are relied upon as a means for driving the correlation between star formation activity and morphology (Springel, Di Matteo & Hernquist 2005; Hopkins et al. 2006). However, our results suggest that mergers, which occur preferentially in group-like environments or the field (McIntosh et al. 2008; Fakhouri & Ma 2008; Darg et al. 2010; Lin et al. 2010), are unlikely to be responsible for the properties of quenched satellites in passive galaxy haloes. Instead, whatever mechanism(s) is responsible for shaping the morphology of our quenched satellite population needs to operate as effectively in the field (i.e. lower-mass haloes) as it does for subhaloes within Milky Way-like systems. While many models suggest that bulge formation is merger-driven (e.g. Toomre 1977; Springel, Di Matteo & Hernquist 2005; Cox et al. 2006), our results would favor a different origin for bulge-dominated morphology (e.g. Kormendy & Kennicutt 2004; Jogee, Scoville & Kenney 2005; MacArthur, Courteau & Holtzman 2003), since we find no variation in Sérsic index with environment. Collectively, our results may support a picture where the cessation of star formation (e.g. via gas removal from ram pressure/strangulation or blow-out) triggers an associated morphological transformation.

Finally, we also examined the dependence of quenching efficiency on projected host/satellite separation, finding a radial gradient in the conversion fraction,  $f_{\text{convert}}^x$ , around passive galaxies. Recent work by Kauffmann et al. (2013) reports a correlation in the specific SFR of satellites extending out to comparable spatial scales around massive central galaxies; for hosts with stellar masses of  $>10^{10} M_{\odot}$ , Kauffmann et al. (2013) argue that this correlation is confined to spatial scales less than 1-2 Mpc. Analyzing satellite galaxies around massive ( $\sim 10^{11} M_{\odot}$ ) central galaxies selected from the GAMA project, Prescott et al. (2011) also find a significant radial dependence for the satellite red fraction out to separations of roughly 500 Mpc.

The observed radial trend measured in our sample could reflect a correlation between infall time and the cessation of star formation, such that more-recently accreted satellites are more likely to be star forming (see also Hearin & Watson 2013). However, the connection between infall time and projected distance is particularly poor inside the virial radius (Oman, Hudson & Behroozi 2013). Instead, if the CGM drives the quenching of star formation via ram-pressure stripping or strangulation, the radial dependence of quenching efficiency could be the result of radial variation in the properties of the CGM — a denser CGM would yield more effective gas stripping, as the ram pressure force scales with the density of the stripping medium Gunn & Gott (1972).

Altogether, our study has uncovered two remarkable results with regard to the properties of relatively massive satellite galaxies around  $\sim L^*$  hosts in the local Universe: (i) falling into a  $\sim 10^{12.3} M_{\odot}$  halo hosted by a star forming central galaxy has a negligible impact on the star formation rate of  $\sim 0.1 L^*$  galaxies, such that massive satellites of

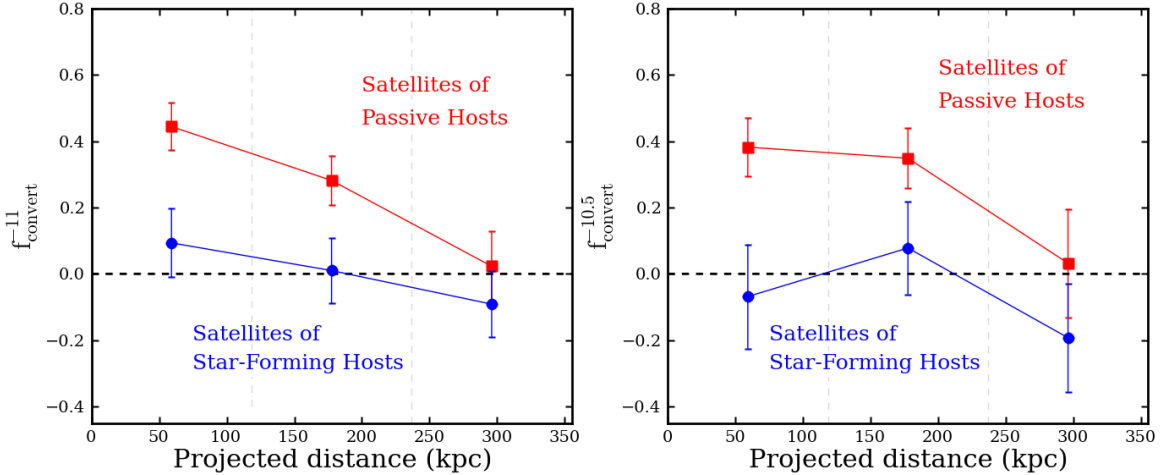


**Figure 9.** Conversion fractions of satellites around passive (red line) and star forming hosts (blue line) as a function of projected distance from the central galaxy. The dashed vertical grey lines denote the edges of the radial bins. (*Left*):  $f_{\text{convert}}^{-11}$ , representative of the fraction of star-forming satellites that have their star formation quenched upon infall. Around star-forming hosts, quenching is only seen at small projected radii, while around passive hosts, quenching is observed out to our radial limit. (*Right*):  $f_{\text{convert}}^{-10.5}$ , representative of the fraction of vigorously star forming satellites that have their star formation suppressed upon infall. For star forming hosts, the quenching observed in the left panel is no longer apparent; the frequency of vigorous star forming satellites suppressed around star forming hosts is consistent with the field at all projected radii.

star forming hosts are indistinguishable from a field population of like stellar mass, and (*ii*)  $\sim 30\%$  of star forming galaxies accreted into a similar halo hosting a passive central galaxy are quenched, but with no corresponding change in morphology. When combined, these results support a picture where the mechanism(s) by which bright satellites of  $\sim L^*$  galaxies are quenched only occur in haloes where the central galaxy is itself quenched. This could either imply that the same quenching mechanism is operating on host and satellite, or it could point to a secondary effect, perhaps associated with differences in the CGM of quenched and star forming galaxies. Whatever the quenching mechanism, it impacts the morphologies of satellites in a manner that mirrors distinct quenching mechanisms in the field.

It is worth emphasizing one particularly interesting implication of our findings: even for passive hosts, the quenching mechanism(s) must operate(s) inefficiently (possibly with a long timescale, De Lucia et al. 2012; Wetzel et al. 2013a; Trinh et al. 2013), such that only  $\sim 30\%$  of satellites that have fallen in from the field are quenched. This relatively low quenching efficiency is mirrored in studies of lower-mass satellites (Geha et al. 2012). It is not clear why quenching occurs around passive hosts (and not star forming hosts) but the fact that it is apparently fairly inefficient may be a clue to its origin. Moreover, while our results focus on fairly massive satellites ( $M_* > 10^{9.5} M_\odot$ ), we know from studies of dwarf galaxies in the Local Group that quenching must become very efficient for smaller satellites. The vast majority of low-mass satellites ( $M_* < 10^8 M_\odot$ ) within the virial radii of the Milky Way and M31 are gas-poor and quenched, in contrast to the field population (McConnachie 2012). Our ongoing work involves investigating this potential mass dependence along with the exploration of simple quenching models that can replicate the relatively inefficient quenching of massive satellites (Wheeler et al., in prep).

## 6 CONCLUSIONS

In this work, we have investigated quenching and suppression of star formation of satellite galaxies in the mass range  $10^{9.5} M_\odot < M_* < 10^{10.5} M_\odot$  orbiting hosts that are selected to have  $M_* > 10^{10.5} M_\odot$ . Our hosts are chosen to be central galaxies of  $\sim 10^{12.3} M_\odot$  dark matter haloes, selected via careful isolation criteria to the group and cluster environment. In order to evaluate the degree of quenching among satellite systems, we make comparisons to stellar-mass matched control samples of isolated, low-mass field galaxies.

Our key result (Figure 7) is that there is a dichotomy in satellite quenching based on host star formation strength: passive hosts quench roughly 30% of their infalling satellites, while satellites of star forming hosts of the same stellar mass show a SSFR distribution consistent with field galaxies. Around passive galaxies, quenching is only present in the inner  $\sim 200$  kpc, significantly less than the virial radius of these hosts, and increases in efficiency with decreasing host/satellite separation. We also show that passive satellites and passive field galaxies show no morphological distinction at fixed stellar mass.

This paper presents a clear dichotomy in massive satellite quenching; however, we anticipate that other trends will be present. For example, smaller ( $M_* < 10^8 M_\odot$ ) satellites in the Local Group are universally quenched, suggesting that quenching might be related to satellite stellar mass. We will explore trends with host and satellite stellar mass in a companion paper.

## ACKNOWLEDGMENTS

This work was supported in part by NSF grants AST-1009973 and AST-10999 and NASA grant NNX09AD09G. MB-K acknowledges support from the Southern California

Center for Galaxy Evolution, a multicampus research program funded by the University of California Office of Research. The Millennium-II simulation database used in this paper and the web application providing online access to them were constructed as part of the activities of the German Astrophysical Virtual Observatory. EJT acknowledges support for this work provided by NASA through Hubble Fellowship grant #HF-51316.01, awarded by the Space Telescope Science Institute, which is operated by the Association of Universities for Research in Astronomy, Inc., for NASA, under contract NAS 5-26555.

Funding for the SDSS and SDSS-II has been provided by the Alfred P. Sloan Foundation, the Participating Institutions, the National Science Foundation, the U.S. Department of Energy, the National Aeronautics and Space Administration, the Japanese Monbukagakusho, the Max Planck Society, and the Higher Education Funding Council for England. The SDSS Web Site is <http://www.sdss.org/>.

The SDSS is managed by the Astrophysical Research Consortium for the Participating Institutions. The Participating Institutions are the American Museum of Natural History, Astrophysical Institute Potsdam, University of Basel, University of Cambridge, Case Western Reserve University, University of Chicago, Drexel University, Fermilab, the Institute for Advanced Study, the Japan Participation Group, Johns Hopkins University, the Joint Institute for Nuclear Astrophysics, the Kavli Institute for Particle Astrophysics and Cosmology, the Korean Scientist Group, the Chinese Academy of Sciences (LAMOST), Los Alamos National Laboratory, the Max-Planck-Institute for Astronomy (MPIA), the Max-Planck-Institute for Astrophysics (MPA), New Mexico State University, Ohio State University, University of Pittsburgh, University of Portsmouth, Princeton University, the United States Naval Observatory, and the University of Washington.

The authors wish to thank Betsy Barton for her support and contributions to this work, and wish to thank the anonymous referee for their helpful comments.

## REFERENCES

- Abazajian K. N. et al., 2009, *ApJS*, 182, 543  
 Baldry I. K., Glazebrook K., Brinkmann J., Ivezić Ž., Lupton R. H., Nichol R. C., Szalay A. S., 2004, *ApJ*, 600, 681  
 Bamford S. P. et al., 2009, *MNRAS*, 393, 1324  
 Barton E. J., Arnold J. A., Zentner A. R., Bullock J. S., Wechsler R. H., 2007, *ApJ*, 671, 1538  
 Behroozi P. S., Conroy C., Wechsler R. H., 2010, *ApJ*, 717, 379  
 Behroozi P. S., Wechsler R. H., Conroy C., 2012, *ArXiv e-prints*  
 Bekki K., 2009, *MNRAS*, 399, 2221  
 Bell E. F., McIntosh D. H., Katz N., Weinberg M. D., 2003, *ApJS*, 149, 289  
 Bell E. F. et al., 2012, *ApJ*, 753, 167  
 Binney J., 1977, *ApJ*, 215, 483  
 Birnboim Y., Dekel A., 2003, *MNRAS*, 345, 349  
 Blanton M. R. et al., 2003, *AJ*, 125, 2348  
 Blanton M. R., Eisenstein D., Hogg D. W., Schlegel D. J., Brinkmann J., 2005a, *ApJ*, 629, 143  
 Blanton M. R. et al., 2005b, *AJ*, 129, 2562  
 Boylan-Kolchin M., Springel V., White S. D. M., Jenkins A., Lemson G., 2009, *MNRAS*, 398, 1150  
 Brinchmann J., Charlot S., White S. D. M., Tremonti C., Kauffmann G., Heckman T., Brinkmann J., 2004, *MNRAS*, 351, 1151  
 Bryan G. L., Norman M. L., 1998, *ApJ*, 495, 80  
 Cheung E. et al., 2012, *ApJ*, 760, 131  
 Cooper M. C. et al., 2010a, *MNRAS*, 409, 337  
 Cooper M. C., Gallazzi A., Newman J. A., Yan R., 2010b, *MNRAS*, 402, 1942  
 Cooper M. C. et al., 2006, *MNRAS*, 370, 198  
 Cox T. J., Dutta S. N., Di Matteo T., Hernquist L., Hopkins P. F., Robertson B., Springel V., 2006, *ApJ*, 650, 791  
 Darg D. W. et al., 2010, *MNRAS*, 401, 1552  
 Davé R., Oppenheimer B. D., Finlator K., 2011, *MNRAS*, 415, 11  
 De Lucia G., Weinmann S., Poggianti B. M., Aragón-Salamanca A., Zaritsky D., 2012, *MNRAS*, 423, 1277  
 Driver S. P. et al., 2011, *MNRAS*, 413, 971  
 Edman J. P., Barton E. J., Bullock J. S., 2012, *MNRAS*, 424, 1454  
 Elbaz D. et al., 2007, *A&A*, 468, 33  
 Fakhouri O., Ma C.-P., 2008, *MNRAS*, 386, 577  
 Geha M., Blanton M. R., Yan R., Tinker J. L., 2012, *ApJ*, 757, 85  
 Gunn J. E., Gott, III J. R., 1972, *ApJ*, 176, 1  
 Guo Q. et al., 2011, *MNRAS*, 413, 101  
 Guo Q., White S., Li C., Boylan-Kolchin M., 2010, *MNRAS*, 404, 1111  
 Hearin A. P., Watson D. F., 2013, *ArXiv e-prints*  
 Hogg D. W. et al., 2004, *ApJ*, 601, L29  
 Hopkins P. F., Hernquist L., Cox T. J., Di Matteo T., Robertson B., Springel V., 2006, *ApJS*, 163, 1  
 Humphrey P. J., Buote D. A., Canizares C. R., Fabian A. C., Miller J. M., 2011, *ApJ*, 729, 53  
 Humphrey P. J., Buote D. A., O’Sullivan E., Ponman T. J., 2012, *ApJ*, 755, 166  
 Jogee S., Scoville N., Kenney J. D. P., 2005, *ApJ*, 630, 837  
 Kauffmann G. et al., 2003, *MNRAS*, 341, 54  
 Kauffmann G., Li C., Zhang W., Weinmann S., 2013, *MNRAS*, 430, 1447  
 Kawata D., Mulchaey J. S., 2008, *ApJ*, 672, L103  
 Kereš D., Katz N., Fardal M., Davé R., Weinberg D. H., 2009, *MNRAS*, 395, 160  
 Kereš D., Katz N., Weinberg D. H., Davé R., 2005, *MNRAS*, 363, 2  
 Kimm T. et al., 2009, *MNRAS*, 394, 1131  
 Klypin A. A., Trujillo-Gomez S., Primack J., 2011, *ApJ*, 740, 102  
 Komatsu E. et al., 2011, *ApJS*, 192, 18  
 Kormendy J., Kennicutt, Jr. R. C., 2004, *ARA&A*, 42, 603  
 Larson R. B., Tinsley B. M., Caldwell C. N., 1980, *ApJ*, 237, 692  
 Leauthaud A. et al., 2012, *ApJ*, 744, 159  
 Lin L. et al., 2010, *ApJ*, 718, 1158  
 MacArthur L. A., Courteau S., Holtzman J. A., 2003, *ApJ*, 582, 689  
 Mandelbaum R., Seljak U., Kauffmann G., Hirata C. M., Brinkmann J., 2006, *MNRAS*, 368, 715  
 Martig M., Bournaud F., Teyssier R., Dekel A., 2009, *ApJ*, 707, 250

- McConnachie A. W., 2012, *AJ*, 144, 4
- McIntosh D. H., Guo Y., Hertzberg J., Katz N., Mo H. J., van den Bosch F. C., Yang X., 2008, *MNRAS*, 388, 1537
- Moster B. P., Naab T., White S. D. M., 2013, *MNRAS*, 428, 3121
- Mulchaey J. S., Jeltama T. E., 2010, *ApJ*, 715, L1
- Noeske K. G. et al., 2007, *ApJ*, 660, L43
- Oman K. A., Hudson M. J., Behroozi P. S., 2013, *MNRAS*, 431, 2307
- O’Sullivan E., Forbes D. A., Ponman T. J., 2001, *MNRAS*, 328, 461
- Peng Y.-j., Lilly S. J., Renzini A., Carollo M., 2012, *ApJ*, 757, 4
- Prescott M. et al., 2011, *MNRAS*, 417, 1374
- Rees M. J., Ostriker J. P., 1977, *MNRAS*, 179, 541
- Robotham A. S. G. et al., 2013, *MNRAS*, 431, 167
- Salim S. et al., 2007, *ApJS*, 173, 267
- Sérsic J. L., 1968, *Atlas de galaxies australes*
- Somerville R. S., Hopkins P. F., Cox T. J., Robertson B. E., Hernquist L., 2008, *MNRAS*, 391, 481
- Springel V., Di Matteo T., Hernquist L., 2005, *ApJ*, 620, L79
- Stewart K. R., Kaufmann T., Bullock J. S., Barton E. J., Maller A. H., Diemand J., Wadsley J., 2011, *ApJ*, 735, L1
- Strateva I. et al., 2001, *AJ*, 122, 1861
- Sun M., Jones C., Forman W., Vikhlinin A., Donahue M., Voit M., 2007, *ApJ*, 657, 197
- Tollerud E. J., Boylan-Kolchin M., Barton E. J., Bullock J. S., Trinh C. Q., 2011, *ApJ*, 738, 102
- Toomre A., 1977, in *Evolution of Galaxies and Stellar Populations*, Tinsley B. M., Larson D. Campbell R. B. G., eds., p. 401
- Trinh C. Q., J. B. E., Bullock J. S., Zentner A. R., Wechsler R. H., 2013, *ArXiv e-prints*
- Tumlinson J. et al., 2011, *Science*, 334, 948
- van den Bosch F. C., Aquino D., Yang X., Mo H. J., Pasquali A., McIntosh D. H., Weinmann S. M., Kang X., 2008, *MNRAS*, 387, 79
- Wang W., White S. D. M., 2012, *MNRAS*, 424, 2574
- Weinmann S. M., Kauffmann G., von der Linden A., De Lucia G., 2010, *MNRAS*, 406, 2249
- Weinmann S. M., Pasquali A., Oppenheimer B. D., Finlator K., Mendel J. T., Crain R. A., Macciò A. V., 2012, *MNRAS*, 426, 2797
- Weinmann S. M., van den Bosch F. C., Yang X., Mo H. J., 2006, *MNRAS*, 366, 2
- Wetzel A. R., Tinker J. L., Conroy C., van den Bosch F. C., 2013a, *MNRAS*, 432, 336
- Wetzel A. R., Tinker J. L., Conroy C., van den Bosch F. C., 2013b, *ArXiv e-prints*
- Wuyts S. et al., 2011, *ApJ*, 742, 96
- Yang X., Mo H. J., van den Bosch F. C., Pasquali A., Li C., Barden M., 2007, *ApJ*, 671, 153
- York D. G. et al., 2000, *AJ*, 120, 1579